

This manuscript has been authored by UT-Battelle, LLC under Contract No. DE-AC05-00OR22725 with the U.S. Department of Energy. The United States Government retains and the publisher, by accepting the article for publication, acknowledges that the United States Government retains a non-exclusive, paid-up, irrevocable, world-wide license to publish or reproduce the published form of this manuscript, or allow others to do so, for United States Government purposes. The Department of Energy will provide public access to these results of federally sponsored research in accordance with the DOE Public Access Plan (<http://energy.gov/downloads/doe-public-access-plan>).

In-situ Metal Binder-phase Formation to Make WC-FeNi Cermets with Spark Plasma Sintering from WC, Fe, Ni, and carbon powders

Corson L. Cramer^{1,*}, Alexander D. Preston², Kaka Ma^{2,3}, Peeyush Nandwana⁴

¹Energy & Transportation Science Division, Energy and Environmental Sciences Directorate, Oak Ridge National Laboratory, Oak Ridge, TN, USA

²School of Advanced Materials Discovery, Colorado State University, Fort Collins, CO 80523, USA

³Department of Mechanical Engineering, Colorado State University, Fort Collins, CO 80523, USA

⁴Materials Science and Technology Division, Physical Sciences Directorate, Oak Ridge National Laboratory, Oak Ridge, TN, USA

*cramercl@ornl.gov

Abstract

High-density WC-FeNi ceramic-metal (cermet) composites were fabricated using liquid-phase spark plasma sintering/field-assisted sintering technology (SPS/FAST) with *in-situ* formation of metal binder phase. The precursor materials were micron-sized powders of WC, Fe, Ni, and C. A low melting point from a eutectic reaction of the powders enabled the *in-situ* formation of FeNi alloy and facilitates liquid-phase sintering of the WC. The carbon powder was added to stabilize the formation of the binder phase. Electron backscatter diffraction (EBSD) was performed to measure grain size and orientation. The composite exhibited a 99% theoretical density and a microstructure consisting of rounded and contiguous WC grains. The average grain size is 10.5 μm . The composite has a maximum hardness of 16.1 GPa. This research provides a fast and cost-effective approach to fabricate hard metals.

Key Words: WC-FeNi; Carbon window; *In-situ* formation; Cermet; Hardmetal

Introduction

Ceramic-metal (cermet) or hardmetal tungsten carbide-cobalt (WC-Co) comprised of less than 15 wt.% Co has been used as cutting tools and wear parts since the early 1930s because of its excellent combination of hardness and fracture toughness [1]–[7]. WC-Co cermet materials have been processed via hot pressing, pressing and sintering, and spark plasma sintering. The particle sizes of WC typically ranged from micron- to nano-scale [8], [9]. Co is a favorable metal binder phase due to its complimentary properties relative to WC and its capability to assist liquid-phase sintering [10]. However, Co is expensive relative to Fe and Ni. The cost of Co is 31.75 USD/lb., Ni is 6.09 USD/lb., and Fe is <1 USD/lb. [11]. Therefore, alternative metal binder materials need to be explored to develop cost-effective composites of WC while maintaining mechanical properties, such as high hardness, comparable to WC-Co composites. One metal binder material system of interest is the Fe-Ni binary alloy, which provides adequate mechanical properties with hardness around 10 GPa and fracture toughness around 15-18 $\text{MPa} \cdot \text{m}^{1/2}$, good corrosion

resistance, and lower costs than Co. Since the amounts of Ni in the Fe are usually very small, it is economic to use FeNi, or form it *in situ*.

Earlier work showed that WC-(Fe-Ni) materials exhibited superior mechanical properties compared to WC-Co. González et al. used liquid-phase sintering to make a WC-(Fe-Ni) composite with a Fe-10 wt.% Ni alloy as the metal binder, and the metal binder content was 10 wt.% of the total cermet. It was found that the WC-(Fe-Ni) composite had a higher fracture toughness than a WC-Co composite containing less than 15 wt.% Co [12]. Kakeshita and Wayman showed how a martensitic Fe-Ni phase can be achieved in the presence of WC and the WC-martensitic FeNi composite also exhibited a fracture toughness that is superior to WC-Co [13]. Other processing methods can generate an austenitic metal binder phase or FeNi₃ intermetallic, and austenitic metal binder phase with WC has mechanical properties comparable to WC-Co. Specifically, a hardness increase was observed by Gao et al. when they sintered a powder mixture of WC, Fe, and Ni powder via hot isostatic pressing, with a total 20 wt.% of the metallic components and a 3:1 Fe:Ni weight ratio [14].

While WC-(Fe-Ni) systems are advantageous in terms of cost saving and mechanical properties compared to WC-Co systems, controlling the alloy composition is still challenging due to the dissolution of WC. Cramer et al. used melt infiltration of Ni into WC/Fe pressed preforms to form stabilized WC-(FeNi) cermet without tooling and found that hardness is comparable to WC-Co, but the microstructure was different with more rounded WC grains [15]. A previous study on the thermodynamics of processing WC with many other metal phases suggests that carbon should be added to FeNi phase to stabilize martensite or to stabilize the narrow carbon window, or the range of carbon contents where a two-phase structure of WC and metal binder is obtained. If the carbon window is missed, the formation of ternary or carbon phases can occur [16]. The carbon addition stabilized the carbon window during dissolution and liquid phase sintering of the composite [17]. In terms of chemical composition, best properties were achieved when 12 wt.% of Fe-Ni metallic component was added with 10 wt.% of Ni in the metallic component [16], so that is the composition used in the current research plus addition of carbon.

In the current research, Spark Plasma Sintering/Field Assisted Sintering (SPS/FAST) is used to liquid-phase sinter WC with Fe and form FeNi *in-situ* by starting with micron-sized WC, Fe, Ni, and carbon powder. SPS/FAST is a method to consolidate powders like hot pressing, but the conduction of electrical current goes through the die and sometimes the sample (if the sample is conductive) resulting in much faster processing than hot pressing and inducing some electric fields on the specimens during processing [18]–[20]. Using SPS/FAST improves processing times because the processing is up to 20 times faster than pressing and sintering. Also, the raw materials can be blended together, so there is no need to use alloys, which can be more expensive and more difficult to process. The raw materials create the melt for liquid-phase sintering and stabilize the final phase *in situ* around the WC. The combination of using raw materials, cheaper materials, *in-situ* formation, and a fast processing method reduces the costs of making this material significantly, and it has not been done this way previously. The drawbacks are small batch sizes and simple geometries. The SPS/FAST method with cost-effective metal binder

phase provides a fast fabrication method of WC hardmetal with low-cost metal binder phase material exhibiting high hardness, and contiguous microstructure.

Materials and Methods

Stoichiometric WC powder (-325 mesh, D_{50} ~12 micron) from AEE, Fe powder (1-10 micron, D_{50} ~8 micron) from Atlantic Equipment Engineers (AEE), Nickel powder (-325 mech, D_{50} ~30 micron) from Alfa Aesar, Carbon black from Nuchar were used for preforms. The WC was blended with the metal precursor so that the blend consists of 88 wt.% WC and 12 wt.% metal precursors. The metal precursors were comprised of 89.5 wt.% Fe, 10 wt.% Ni, and 0.5 wt.% Scanning Electron Microscopy (SEM) and Horiba LA-950 laser scatter particle distribution analysis on the powder was done and is the same as [21]. The particles show a wide distribution range from about 6-40 micrometers. Most of the particles exhibit spherical morphology, with a few particles showing irregular shapes.

5 g of the mixed WC/Fe/Ni/carbon powder was pressed at 5 MPa for 1 min in a graphite die of 20 mm diameter before sintering. Graphite punches were machined to a tight fit tolerance with the 20 mm die, and sample thicknesses were 2-3 mm after sintering. The heating schedule was 1050°C at 100°C/min with 5-minute hold in vacuum while holding 50 MPa pressure on the graphite punches with a Thermal Technology Spark Plasma Sintering Machine 25-10. A densification curve was constructed using the green density, final density, and displacement data. The samples were extracted from the dies after sintering with a hand-cranked press. Upon unloading the sample, the die was cracked. There was some metallic material that segregated from the sintering sample and deposited on the graphite punch and die wall. This makes the die sacrificial and adds to costs.

The specimen microstructures were analyzed with SEM using a Hitachi S4800 microscope in backscatter electron imaging mode. Bulk and Archimedes densities were measured when appropriate by measuring the part dimensions, dry mass, and submerged mass. Areal density was measured using ImageJ software to analyze SEM images of cross-section microstructure. Crystallographic phase composition was determined by x-ray diffraction (XRD) using a PANalytical X'pert diffractometer with Mo K- α radiation ($\lambda = 0.709319 \text{ \AA}$). The operating parameters were 40 kV and 40 mA, with a 2θ step size of 0.0167 °/sec. The XRD patterns were analyzed using the whole pattern fitting approach with MDI Jade 2010 software database. Differential thermal analysis (DTA) was performed with a Netzsch STA 449 F3 Jupiter simultaneous thermal analyzer in an argon atmosphere to identify thermodynamic activity during processing. DTA scans were performed at ambient pressure with heating rate of 10°C/min. Vickers hardness measurements were performed using a LECO LM 110AT apparatus under a 1.0 kgf load. Electron backscatter diffraction (EBSD) analysis was done on the microstructure to measure grain size and orientation.

Results and Discussion

Figure 1 shows XRD patterns of the precursor powder and the sintered sample. The powder had distinct peaks for WC, Fe, and Ni, but not for carbon as carbon content is only 0.5 wt.% of the metal binder, which is less than the detection limit of any XRD device. In contrast, the sintered

sample exhibit peaks for WC and ferrite Fe (BCC α -Fe) only, indicating that Ni is in complete solid solution with Fe and the Fe retained its original crystal structure as the precursor.

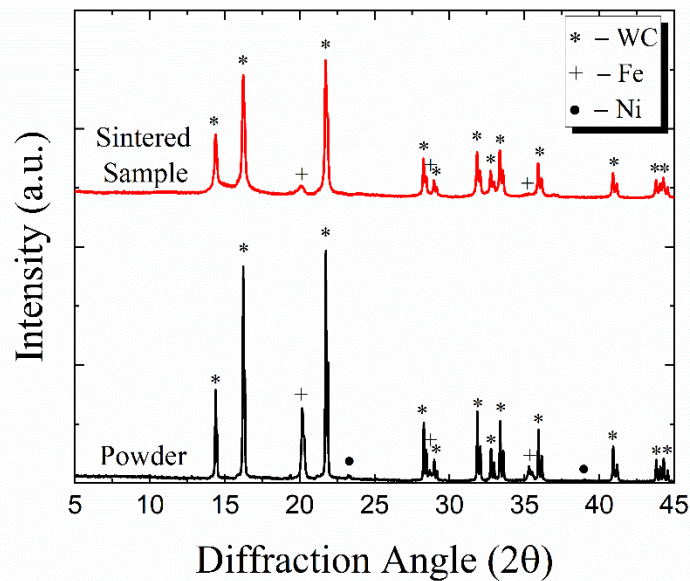


Figure 1: XRD patterns of the precursor powders and sintered sample.

Figure 2 shows the sample density and applied mechanical pressure as a function of the sintering time. Table 1 provides the green and final density values of the sample. The density calculated on the sintering curve in Figure 2 was derived based on knowing the green, final density, and the measured displacement. The powder compact started at 50 %TD as measured by bulk measurements using mass and geometric volume of the sample. The densification curve showed the behavior of the powder during sintering as function of temperature. The powder densified differently at three stages. When the temperature increased from 300°C to 550°C, the pressure was held constant, but the density increased. This densification most likely resulted from stage one sintering where rearrangement of particles occurred, and particle necking formed due to surface diffusion. When the temperature increased from 550 to 700°C, the pressure was ramped from 15 MPa to 50 MPa, the density increased likely due to closer packing of the powder from the pressure increase. From 700°C to 900°C, little to no further densification was observed. From 900°C to 1050°C, there is a large amount of densification, which was most likely from liquid-phase sintering mechanisms. There was some densification during the 5 min hold, which enabled the powder to reach near full density of 99% theoretical density (TD).

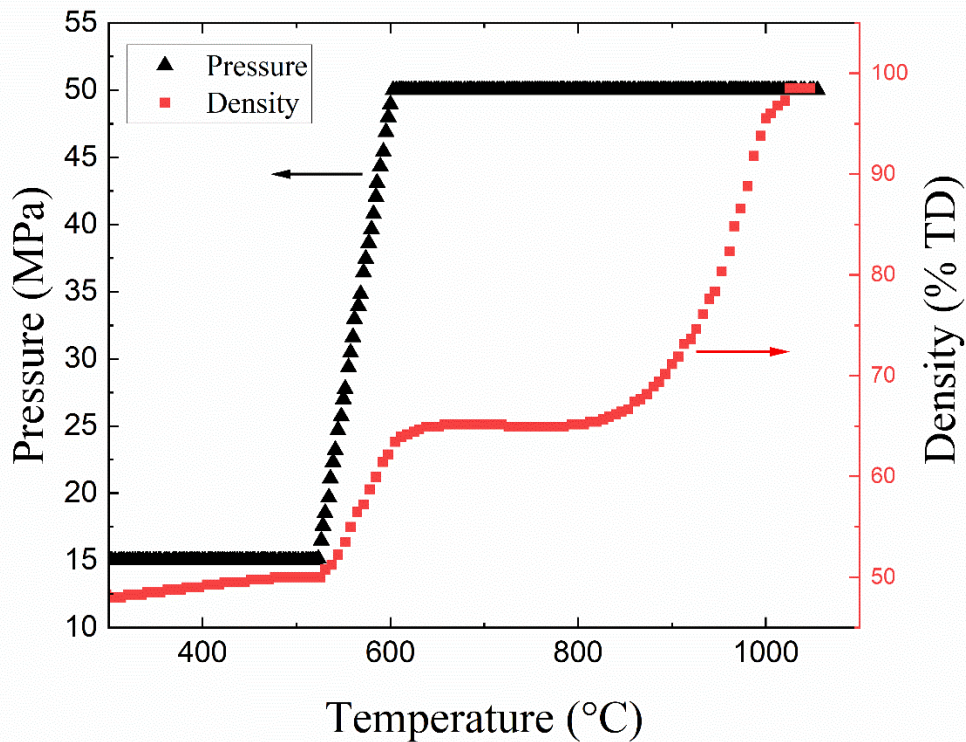


Figure 2: Plot of density and applied mechanical pressure on the graphite punches versus temperature upon heating of the powder during sintering.

Figure 3 shows DTA data of the powder blend upon heating. The heating was done without pressure and at a slower rate due to machine capability. Though it was not the best comparison to isolate any kinetic effect, it does represent the thermodynamics accurately to identify reactions such as phase transformation and melting. A distinct endothermic peak was observed at 1275°C, which corresponds to the eutectic point reached in the powder during heating. The maximum temperature measured during SPS was 1050°C, lower than the eutectic point, 1275°C, identified by the DTA. Yet the density of the sintered sample suggested sintering occurred. The prominent type of sintering of WC with metals in which WC is soluble at this temperature is liquid-phase sintering [22], [23]. The discrepancy between sintering temperature and eutectic point resulted from the difference between the temperature measured by a thermal couple positioned at the die hole and the actual temperature reached in the powder, which was typically higher than the former. In addition, a radially graded thermal distribution may exist during SPS, which makes the center of the specimen hotter than the outer parts [24]. As a result, local melting of the metallic powder occurred and contributed to the liquid-phase sintering. Other studies have reported a lower eutectic point, 1085°C, for FeNi system, which is closer to 1050°C used in the current research [25], [26].

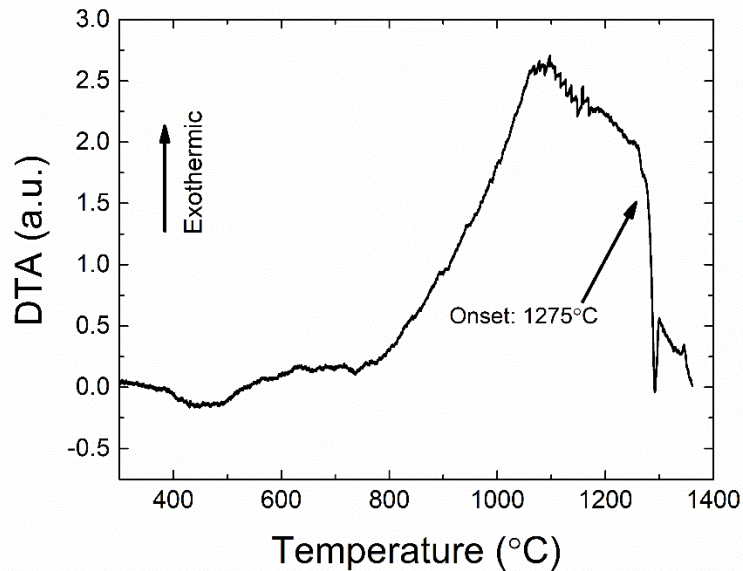


Figure 3: DTA data of the WC, Fe, Ni, and carbon powders heated to 1400°C. Heating shows thermodynamic action during heating, and the powders display an endothermic reaction at 1275°C, which is associated with a melting event.

Figure 4 shows and characterizes the microstructure of cross-sections of the sample via optical imaging, SEM, and EDS. The density of the sintered sample reaches 99 %TD, despite of very few pores and defects, highlighted by the black arrows in Fig. 4a. The density values are provided in Table 1. In the SEM images, the black shade is the FeNi phase, and the light and dark grey shades are WC grains, and the different shades are most likely different grain orientations. The SEM of the spot near the surface of the sample shows higher WC content than center of the sample. The corresponding EDS shows W is separated from Fe. It is typically difficult to detect light element such as carbon in EDS [27], [28]. Therefore, the separation of W and Fe in the EDS mapping indicates that the WC particles are surrounded by Fe. The Ni content (~ 1.2 wt.% of the total composite) is too small to be detected in EDS. XRD patterns suggest Ni is most likely in solid solution with the Fe. The center of the samples shows a higher wt.% of Fe, suggesting that some of the metal binder migrated to the middle of the sample or some of the WC migrated to the top of the sample. The average hardness of the sample was 16.1 ± 1.2 GPa near the edge where the WC content is higher and 13.2 ± 1.3 GPa near in the center where the WC content is slightly lower, as shown in Table 1, which is indicative of the high-density cermet material with high WC content where WC-Co values are around 12-15 GPa for similar grain size and metal binder wt.% [1], [5], [9]. The microstructure showed more rounding of WC particles versus the typical sharp, faceted, and contiguous grains in WC-Co hardmetal [17], [29]. The difference in the WC phase morphology probably results from the different dissolution rate of WC into liquid Fe-Ni melt compared to Co, and this same morphology of WC grains, more circular than faceted, was also seen in Cramer et al. [15].

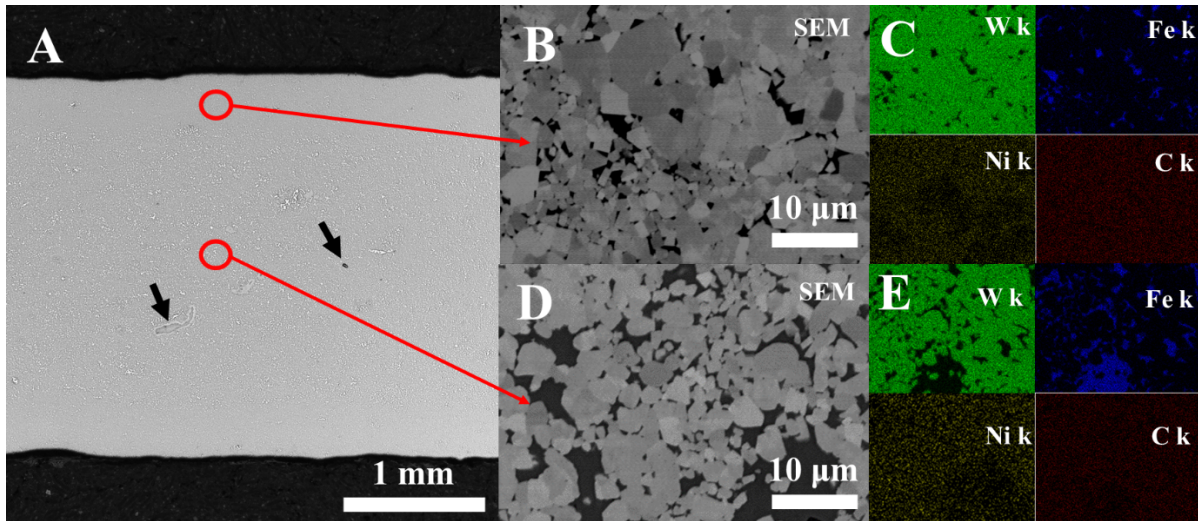


Figure 4: A) Optical image of a cross-section of the composite sample, B) SEM of spot near the edge, C) EDS of the spot on the edge, D) SEM of the spot in the center of the cross-section, and E) EDS of the spot in the center of the cross-section.

Figure 5 shows the EBSD data from a spot in between the two SEM spots. It shows grain size and orientation mapping with an inverse pole figure (IPF) and texture plot. The average grain size is $10.5 \pm 3.2 \mu\text{m}$. No specific texture is observed. The maximum texture intensity was roughly 3.1. There is not enough metal binder phase in some sections to get enough confidence index with EBSD, which is commonly reported in other studies [30], [31]. Therefore, the EBSD scans were indexed with only WC.

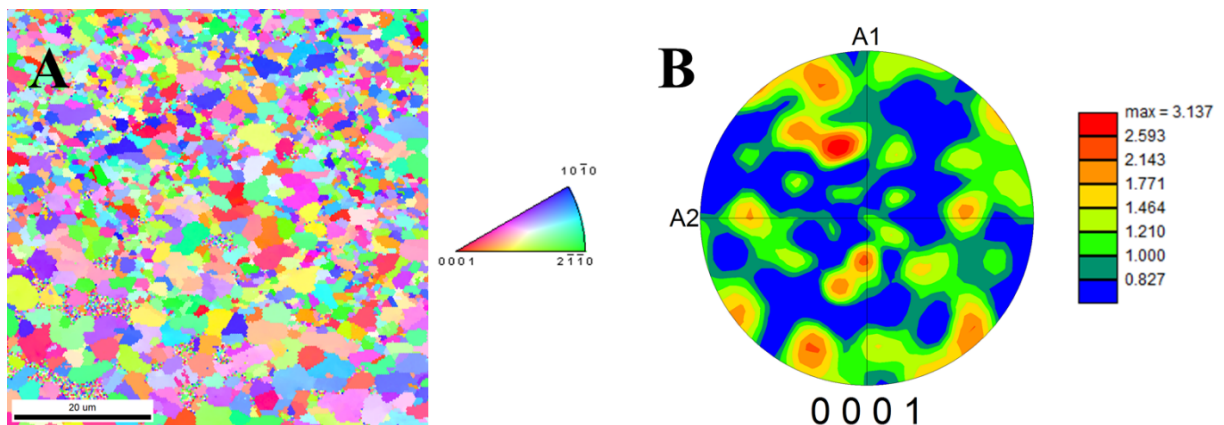


Figure 5: A) Inverse pole figure and B) associated $\langle 0001 \rangle$ pole figure of the sintered WC-(Fe-Ni-C) sample showing a lack of specific texture.

Table 1: Densities, hardness, and grain size of samples processed with SPS at 1050°C.

Property	Results
Green density	7.0 g/cm ³ , 50 %TD
Sintered density (g/cm ³ , %TD)	13.8 g/cm ³ , 99 %TD
Hardness on outer part	16.1 ± 1.2 GPa
Hardness on inner part	13.2 ± 1.3 GPa
Grain size from EBSD	10.5 ± 3.2 μm

Dense WC cermet was manufactured using SPS/FAST with a more cost-effective alloy compared to WC. The alloy is known to behave like Co during processing and have similar properties. Also, the powder size and final grain size is micron-sized, which makes manufacturing more cost-effective and safer. Making the composite *in situ* has not been done before but was achieved here and adds to lowering costs of production because raw materials can be used. The material first reached a point where the entire sample is partially liquid during processing. The melt then aided in liquid-phase sintering of the WC and made solid solution FeNi alloy *in situ* in one step. The composite materials made here can be used as cutting tools with minimal extra machining. The FeNi phase is stabilized throughout the WC, and the WC grains are more circular compared to faceted WC grain when using Co as the binder phase metal. The effects of carbon are not understood, but carbon is used to make the alloy *in situ*. It is thought that the carbon is needed, but this can be tested and compared to density and microstructure of the current research. More mechanical properties such as fracture toughness can be tested and compared to the typical WC-Co. More complex shapes can be made with triangular dies and punches.

Conclusion

Dense hardmetal samples were made with SPS/FAST starting with WC, Fe, Ni, and C precursor powders creating the metal binder phase *in situ*. The use of SPS/FAST reduces processing time significantly and allows for high WC content consolidation with large powders by using an apparent eutectic point during processing, which lowers processing temperature and forms solid solution of the metal binder phase. The formation of *in situ* melt forms a metal binder phase that has high hardness and highly contiguous microstructure. Also, it is more cost-effective than using Co. The density and hardness were 99%TD and 16.1 GPa, respectively. EBSD shows no specific texture, and it also reveals an average grain size of 10.5 μm. The rounding of the particles is thought to be due to less dissolution of the WC into molten Fe. In summary, the hardmetal is a low-cost alternative to WC-Co hardmetal with high hardness.

Acknowledgements

The authors would like to thank Olivia Shafer for editing assistance. This material is based upon work supported by the U.S. Department of Energy, Office of Energy Efficiency and Renewable Energy, Office of Advanced Manufacturing, under contract number DE-AC05-00OR22725.

References

- [1] Y. . Milman, S. Luyckx, and I. Northrop, "Influence of temperature, grain size and cobalt content on the hardness of WC–Co alloys," *Int. J. Refract. Met. Hard Mater.*, vol. 17, no. 1–3, pp. 39–44, May 1999.
- [2] I. Konyashin, S. Hlawatschek, B. Ries, F. Lachmann, and M. Vukovic, "Cobalt capping on WC–Co hardmetals. Part I: A mechanism explaining the presence or absence of cobalt layers on hardmetal articles during sintering," *Int. J. Refract. Met. Hard Mater.*, vol. 42, pp. 142–150, Jan. 2014.
- [3] J. Gurland and T. J. Norton, "Role of binder phase in cemented tungsten carbide-cobalt alloys," *Metals (Basel)*, vol. 194, no. 10, pp. 1051–56, 1952.
- [4] R. K. Viswanadham and P. G. Lindquist, "Transformation-toughening in cemented carbides: Part I. Binder composition control," *Metall. Trans. A*, vol. 18, no. 12, pp. 2163–2173, Dec. 1987.
- [5] J. Gurland and P. Bardzil, "Relation of Strength, Composition, and Grain Size of Sintered WC-Co Alloys," *JOM*, vol. 7, no. 2, pp. 311–315, Feb. 1955.
- [6] T. Kagnaya, C. Boher, L. Lambert, M. Lazard, and T. Cutard, "Wear mechanisms of WC–Co cutting tools from high-speed tribological tests," *Wear*, vol. 267, 2009.
- [7] S. G. Bailey and C. M. Perrott, "Wear processes exhibited by WC-Co rotary cutters in mining," *Wear*, vol. 29, no. 1, pp. 117–128, Jul. 1974.
- [8] S. I. Cha, S. H. Hong, and B. K. Kim, "Spark plasma sintering behavior of nanocrystalline WC–10Co cemented carbide powders," *Mater. Sci. Eng. A*, vol. 351, no. 1–2, pp. 31–38, Jun. 2003.
- [9] W. Su, Y. Sun, H. Wang, X. Zhang, and J. Ruan, "Preparation and sintering of WC–Co composite powders for coarse grained WC–8Co hardmetals," *Int. J. Refract. Met. Hard Mater.*, vol. 45, pp. 80–85, Jul. 2014.
- [10] K. Kudaka and H. Koono, "High-Pressure Sintering of WC Powder and WC–Co Mixed Powder," *Trans. Japan Inst. Met.*, vol. 8, no. 3, pp. 207–208, 1967.
- [11] "Commodity and Metal Prices, Metal Price Charts - InvestmentMine." [Online]. Available: <http://www.infomine.com/investment/metal-prices/>. [Accessed: 11-Jan-2019].
- [12] R. González, J. Echeberría, J. M. Sánchez, and F. Castro, "WC-(Fe,Ni,C) hardmetals with improved toughness through isothermal heat treatments," *J. Mater. Sci.*, vol. 30, no. 13, pp. 3435–3439, 1995.
- [13] T. Kakeshita and C. . Wayman, "Martensitic transformations in cermets with a metastable austenitic binder I: WC-(Fe-Ni-C)," *Mater. Sci. Eng. A*, vol. 141, no. 2, pp. 209–219, Aug. 1991.

- [14] Y. Gao, B.-H. Luo, Z.-H. Bai, B. Zhu, and S. Ouyang, "Effects of deep cryogenic treatment on the microstructure and properties of WC—Fe—Ni cemented carbides," *RMHM*, vol. 58, pp. 42–50, 2016.
- [15] C. L. Cramer, A. D. Preston, A. M. Elliott, and R. A. Lowden, "Highly dense, inexpensive composites via melt infiltration of Ni into WC/Fe preforms," *Int. J. Refract. Met. Hard Mater.*, vol. 82, pp. 255–258, Aug. 2019.
- [16] C. M. Fernandes and A. M. R. Senos, "Cemented carbide phase diagrams: A review," *Int. J. Refract. Met. Hard Mater.*, vol. 29, no. 4, pp. 405–418, Jul. 2011.
- [17] W. D. Schubert, M. Fugger, B. Wittmann, and R. Useldinger, "Aspects of sintering of cemented carbides with Fe-based binders," *Int. J. Refract. Met. Hard Mater.*, vol. 49, pp. 110–123, Mar. 2015.
- [18] O. Guillon *et al.*, "Field-Assisted Sintering Technology/Spark Plasma Sintering: Mechanisms, Materials, and Technology Developments," *Adv. Eng. Mater.*, vol. 16, no. 7, pp. 830–849, Jul. 2014.
- [19] A. Bellosi, F. Monteverde, and D. Sciti, "Fast Densification of Ultra-High-Temperature Ceramics by Spark Plasma Sintering," *Int. J. Appl. Ceram. Technol.*, vol. 3, no. 1, pp. 32–40, Jan. 2006.
- [20] S. Muñoz and U. Anselmi-Tamburini, "Temperature and stress fields evolution during spark plasma sintering processes," *J. Mater. Sci.*, vol. 45, no. 23, pp. 6528–6539, Dec. 2010.
- [21] C. L. Cramer, P. Nandwana, R. A. Lowden, and A. M. Elliott, "Infiltration studies of additive manufacture of WC with Co using binder jetting and pressureless melt method," *Addit. Manuf.*, vol. 28, pp. 333–343, Aug. 2019.
- [22] J.-L. Quenec'h, M. Coster, J.-L. Chermant, and D. Jeulini, "Study of the liquid-phase sintering process by probabilistic models: Application to the coarsening of WC-Co cermets," *J. Microsc.*, vol. 168, no. 1, pp. 3–14, Oct. 1992.
- [23] P. Fan, Z. Z. Fang, and J. Guo, "A review of liquid phase migration and methods for fabrication of functionally graded cemented tungsten carbide," *Int. J. Refract. Met. Hard Mater.*, vol. 36, pp. 2–9, Jan. 2013.
- [24] U. Anselmi-Tamburini, S. Gennari, J. E. Garay, and Z. A. Munir, "Fundamental investigations on the spark plasma sintering/synthesis process," *Mater. Sci. Eng. A*, vol. 394, no. 1–2, pp. 139–148, Mar. 2005.
- [25] A. Antoni-Zdziobek, J. Y. Shen, and M. Durand-Charre, "About one stable and three metastable eutectic microconstituents in the Fe–W–C system," *Int. J. Refract. Met. Hard Mater.*, vol. 26, no. 4, pp. 372–382, Jul. 2008.
- [26] S. Zhou and X. Zeng, "Growth characteristics and mechanism of carbides precipitated in WC–Fe composite coatings by laser induction hybrid rapid cladding," *J. Alloys Compd.*, vol. 505, no. 2, pp. 685–691, Sep. 2010.
- [27] F. C. Miguens, M. L. d. Oliveira, R. V. Marins, and L. D. d. Lacerda, "A new protocol to

- detect light elements in estuarine sediments by X-ray microanalysis (SEM/EDS),” *J. Electron Microsc. (Tokyo)*, vol. 59, no. 5, pp. 437–446, Oct. 2010.
- [28] W. Wunderlich, A. H. Foitzik, and A. H. Heuer, “On the quantitative EDS analysis of low carbon concentrations in analytical TEM,” *Ultramicroscopy*, vol. 49, no. 1–4, pp. 220–224, Feb. 1993.
- [29] J. García, V. Collado Ciprés, A. Blomqvist, and B. Kaplan, “Cemented carbide microstructures: a review,” *Int. J. Refract. Met. Hard Mater.*, vol. 80, pp. 40–68, Apr. 2019.
- [30] J. Long *et al.*, “A new type of WC–Co–Ni–Al cemented carbide: Grain size and morphology of γ' -strengthened composite binder phase,” *Scr. Mater.*, vol. 126, pp. 33–36, Jan. 2017.
- [31] K. P. Mingard, B. Roebuck, J. Marshall, and G. Sweetman, “Some aspects of the structure of cobalt and nickel binder phases in hardmetals,” *Acta Mater.*, vol. 59, no. 6, pp. 2277–2290, Apr. 2011.